J Appl Electrochem (2013) 43:911–917
DOI 10.1007/s10800-013-0587-5

RESEARCH ARTICLE

The microstructure and electrochemical properties of boron-doped nanocrystalline diamond film electrodes and their application in non-enzymatic glucose detection

Y. S. Zou · L. L. He · Y. C. Zhang · X. Q. Shi · Z. X. Li · Y. L. Zhou · C. J. Tu · L. Gu · H. B. Zeng

Received: 5 April 2013 / Accepted: 13 July 2013 / Published online: 24 July 2013

Abstract Boron-doped nanocrystalline diamond (BDND) films were deposited on Si(100) by microwave plasma chemical vapor deposition using trimethyl boron as boron source. The surface morphology, microstructure, and electrochemical properties of the BDND films were investigated. Cyclic voltammograms indicated that the BDND film electrode exhibited good reversibility and repeatability of electrode reaction using $[Fe(CN)_6]^{3-/4-}$ as redox couple. The non-enzymatic glucose sensor based on the as-prepared BDND film electrode without any modification was developed, and the selective detection of glucose in alkaline solution containing interference species of ascorbic acid and uric acid was demonstrated. The results showed that glucose can be directly oxidized with a wide linear range and high sensitivity, and selectively detected in the presence of uric acid and ascorbic acid in alkaline solution using the as-prepared BDND film electrode.

Keywords Boron-doped diamond film · Microstructure · Electrochemical properties · Non-enzymatic glucose sensor

1 Introduction

Diamond is a very attractive material in various electronic and micro-electromechanical applications due to its unique combination of outstanding physical and chemical properties, such as wide band-gap, negative electron affinity (NEA), chemical inertness, and extreme hardness and thermal conductivity [1]. In terms of stability, chemical inertness, wide potential window, low background current, and great fouling resistance [2–4], boron-doped diamond film electrodes outperform conventional metal and other carbonaceous materials electrodes, e.g., gold, platinum, and glassy carbon, highly oriented pyrolytic graphite, porous carbon. Combining the extreme intrinsic properties and excellent electrochemical properties, boron-doped diamond film electrode has been widely used in electroanalysis [5], electrochemical pollutant treatment [6], and electrochemical and biomedical sensors [7–9].

The reliable and fast electrochemical determination of glucose is very important in many fields including clinical diagnostics, food industry, and biotechnology as well as in glucose fuel cells. There are two main approaches to develop electrochemical glucose sensors, i.e., enzymatic [10–14] and non-enzymatic sensors [15–23]. Although enzymatic sensors with the enzyme glucose oxidase (GOx) offer reliable results, the most common and major drawback is the lack of stability due to the intrinsic nature of enzyme. The activity of GOx can be easily affected by temperature, pH, humidity, and toxic chemicals [24]. Moreover, a complicated procedure, including functionalization, adsorption, cross-linking, and entrapment is required for the immobilization of GOx on the electrode surfaces to construct the enzymatic sensors, resulting in the decrease of activity of the GOx. However, those disadvantages can be alleviated when using electrochemical approaches for the detection of glucose with non-enzymatic sensors. So far, considerable effort has been made to develop the non-enzymatic sensor that has high sensitivity and stability. For example, the amperometric measurements of glucose based on carbonaceous materials electrode and various metal

Y. S. Zou (✉) · L. L. He · Y. C. Zhang · X. Q. Shi · Z. X. Li · C. J. Tu · L. Gu · H. B. Zeng
School of Materials Science and Engineering, Nanjing University of Science and Technology, Nanjing 210094, Jiangsu, China
e-mail: yshzou75@gmail.com

Y. L. Zhou
Department of Chemistry, Shangqiu Normal University, Shangqiu 476000, Henan, China

nanomaterials including copper, gold, platinum, and nickel, and alloys without using enzymes [25–29] have been explored in alkaline solutions. The metal electrode surface encounters severe poisoning and causes the decrease of activity due to the absorption of the oxidized products during the process of electrochemical oxidation of glucose. In comparison to the transition metal electrode, boron-doped diamond film electrode was reported to be inert for glucose oxidation, and has been regarded as attractive new electrode in recent years in non-enzymatic glucose sensors due to its outstanding electrochemical properties, including stability, simplicity, and reproducibility. The non-enzymatic glucose sensor with high sensitivity and reproducibility based on the as-prepared boron-doped diamond film electrode was constructed [16, 17], and glucose could be directly oxidized and selectively detected in the presence of ascorbic acid (AA) and uric acid (UA) in alkaline solution.

In this paper, highly boron-doped nanocrystalline diamond (BDND) films were prepared by microwave plasma chemical vapor deposition (MWCVD) using trimethyl boron as boron source. The morphology, microstructure, and electrochemical properties of the prepared BDND films were investigated. The non-enzymatic glucose sensor based on BDND film electrode was constructed and then used for the analysis and selective detection of glucose in solutions containing interfering electroactive components, such as AA and UA.

2 Experimental

The un-doped and BDND films were deposited on Si(100) substrate by MWCVD. Prior to deposition, the substrates were ultrasonically abraded for 60 min in a suspension of mixed diamond powders with a grain size of 5 nm and 3 μm in ethanol to obtain a high nucleation density, and then was cleaned. Boron doping was achieved by adding trimethylboron (TMB, diluted by H_2 to 1,000 ppm) to the gas mixture. The plasma was induced in a gas mixture of 10 %CH_4/90 %(H_2 and TMB) with a microwave power of 1,200 W. The total pressure and gas flow rate were controlled at 30 Torr and 200 sccm, respectively. The boron–carbon (B/C) concentration ratio in the feed gas mixture was kept to 3,000 ppm. The substrate temperature measured by an optical pyrometer was maintained at approximately 800 °C, and the deposition time was 8 h. The morphology, phase composition of the un-doped and BDND films were characterized by scanning electron microscopy (SEM, Philips 30 XL FEG), visible (wavelength: 514.5 nm, Renishaw 2000) and UV (wavelength: 244 nm, Renishaw inVia Raman micrscope) Raman spectroscopy.

The electrochemical measurements were performed in a conventional three-electrode cell system using an electrochemical workstation (CHI 660D, Shanghai Chenhua, China). Platinum wire and saturated calomel electrode (SCE) electrode were used as auxiliary electrode and reference electrode, respectively. The as-prepared BDND films were used as working electrodes, and were sonicated successively in isopropanol, acetone, and ultrapure water for 15 min before use. The electrochemical selective detection of glucose at BDND film electrodes in solutions containing interfering electroactive components of AA and UA was explored. The electrolyte solutions were purged with high-purity N_2 gas for 15 min to reduce the level of oxygen dissolved before each electrochemical measurement. D-Glucose was purchased from Beijing Chemical Plant (Beijing, China). UA and AA were from Sigma.

3 Results and discussion

Figure 1 shows the SEM surface and cross-sectional images of the deposited un-doped and BDND films. Uniform films were obtained after growth of 8 h. It can be seen that the surface morphology of the un-doped nanocrystalline diamond film is very smooth and composed of nanograins of a few tens nanometers in size, while the grains gather together forming ball-like clusters with inhomogeneous size for the BDND films, as shown in Fig. 1a, b. The cross-sectional images demonstrated that the deposited BDND film still maintained the column structure and was well adherent. However, the introduction of TMB in the gas mixture resulted in the decrease of film growth rate due to the modification of plasma composition, e.g., the decrease of H/H_2 and CH/H ratio in the plasma, and chemical reaction. Meanwhile, the doped boron atoms also can terminate the growth sites and further inhibit the diamond growth.

Figure 2 shows the visible and UV Raman spectra of nanocrystalline diamond films before and after boron doping. As shown in Fig. 2a, five peaks around 1,140; 1,330; 1,350; 1,470; and 1,560 cm^{-1} in the visible Raman spectra (curve I) were observed for the un-doped nanocrystalline diamond film. The weak diamond characteristic peak ca. 1,330 cm^{-1} is assigned to the crystalline sp^3-hybridized carbon Raman peak. Broadening of the diamond band is a result of diamond grain size decreasing to the nanometer scale. The two peaks at 1,140 and 1,470 cm^{-1} are attributed to the C–H bonds in a transpolyacetylene segments present at the grain boundaries and surfaces of diamond film, indicating the formation of nanocrystalline diamond. The peaks located at about 1,350 and 1,560 cm^{-1} are for the amorphous carbon and graphitic carbon. In the case of BDND film, two peaks around 500 and 1,220 cm^{-1} become the main features in the visible Raman spectra (curve II), which are associated with Fano interference effect as a result of heavy boron doping in nanocrystalline diamond [30]. Furthermore, the diamond characteristic

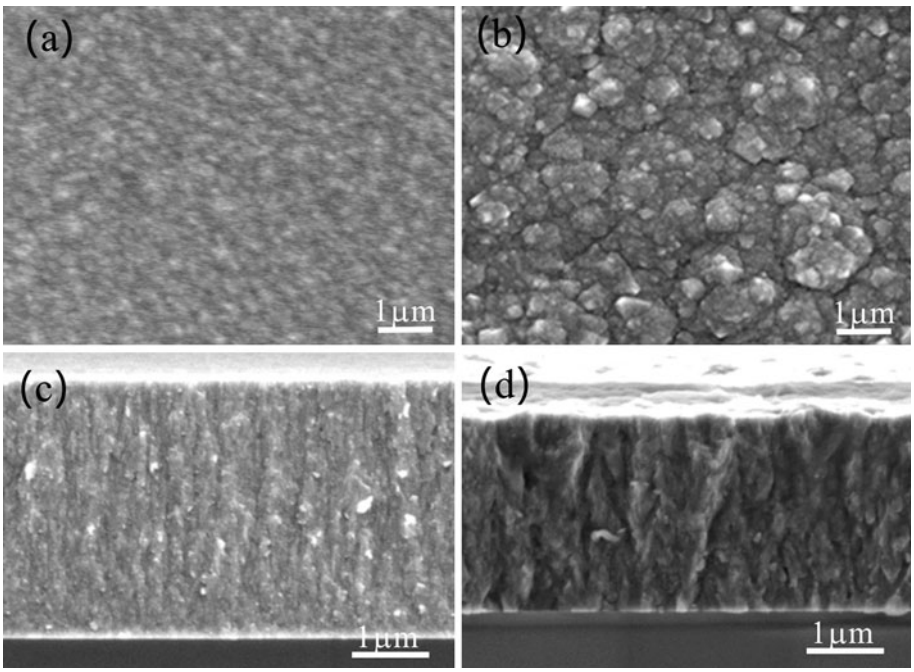

Fig. 1 SEM plain view and cross-sectional image of undoped (**a**) and (**c**), and boron-doped (**b**) and (**d**) nanocrystalline diamond films

peak at 1,332 cm^{-1} downshifted to about 1,320 cm^{-1} and became more asymmetric due to boron doping. According to the empirical equation [31]: $[B]\ cm^{-3} = 8.44 \times 10^{30} \exp(-0.048\omega)$, boron concentration in the diamond film can be evaluated, where ω is the center wavenumber of characteristic peak at about 500 cm^{-1} by fitting this peak with a combination of Gaussian and Lorentzian line shapes. It is calculated that the boron doping level is about 2.0×10^{20} cm^{-3} for the BDND film. In UV Raman spectra, a sharp peak located at 1,332 cm^{-1} and a broad peak located at 1,580 cm^{-1} were observed, as shown in Fig. 2b, which are characteristic to diamond and graphitic carbon, respectively. Unlike to visible Raman, the two peaks located at 500 and 1,220 cm^{-1} were not detected in UV Raman spectra (curve II) for the BDND film. Moreover, the relative intensity of diamond peak decreased after boron doping, which indicated that boron doping resulted in increasing the sp^2 carbon bond content of the BDND film.

Figure 3 shows the cyclic voltammograms (CV) of BDND film electrode in 0.1 M H_2SO_4 electrolyte. For the comparison, the CV measurement of the glassy carbon electrode was also performed. It demonstrated that the electrochemical potential window of BDND film electrode and glassy carbon electrode was about 3.6 and 3.0 V, respectively. Compared to the glassy carbon electrode, the BDND film electrode shows a wider electrochemical potential window. Also, the current for BDND film electrode is significantly less than that for glassy carbon electrode, as shown in the curve I and II. The surface of CVD BDND film was terminated with hydrogen after the film deposition. Due to the hydrophobic surfaces, BDND film electrode reactions that involve adsorbed intermediates can be effectively inhibited on diamond. Thus, the BDND film electrode has a wide electrochemical potential window and the water electrolysis can be negligible within a wide potential range on the BDND diamond electrode. Besides, the anodic oxidation potential of BDND film electrode is about 2.3 V, indicating that most organic pollutants can be directly oxidized and degraded on the surface of BDND film electrode.

The electrochemical behavior of the BDND film electrode was evaluated by the analysis of redox couples of $Fe(CN)_6^{3-/4-}$. Figure 4 shows the CV of 0.2 mM $K_3Fe(CN)_6$ in 1 M KCl solution at the scan rate varying from 25 to 250 mV s^{-1} on BDND film electrode. Well-defined and symmetric CV curves of $[Fe(CN)_6]^{3-}/[Fe(CN)_6]^{4-}$ on the BDND electrode were obtained. The anodic peak potential to cathodic peak potential separations (ΔE_p) for the BDND film electrode at the scan rate of 25 mV s^{-1} is about 70 mV, which indicates that there is a nearly reversible or quasi-reversible electrode reaction of $K_3Fe(CN)_6$ on the surface of BDND film electrode. As the scan rate increased, the peak current of cathodic and anodic increased, while the peak potential separations (ΔE_p) changed slightly. The electrochemical response of $Fe(CN)_6^{3-/4-}$ on the surface of BDND film electrode exhibits a linear relationship between the anodic or cathode peak current and square root of scan rate from 25 to 250 mV s^{-1}, as shown in the inset of Fig. 4, indicating a typical diffusion-controlled process of the electrode reaction of $K_3Fe(CN)_6$.

Figure 5 shows that the CV of 0.2 mM $K_3Fe(CN)_6$ in 1 M KCl solution at the BDND film electrode for successive ten times scanning at the scan rate of 50 mV s^{-1}. It can be seen that ten successive amperometric measurements of 0.2 mM $K_3Fe(CN)_6$ on one BDND film electrode almost coincided with each other and yielded a reproducible current with the

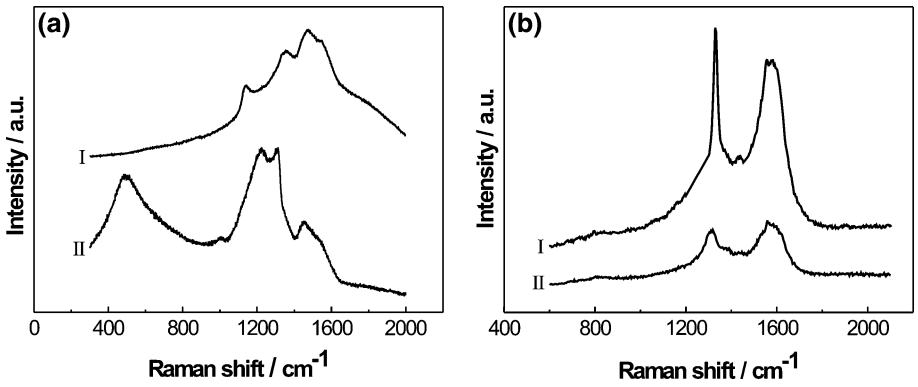

Fig. 2 Visible (**a**) and UV (**b**) Raman spectra acquired from the un-doped (spectrum I) and boron-doped (spectrum II) nanocrystalline diamond films

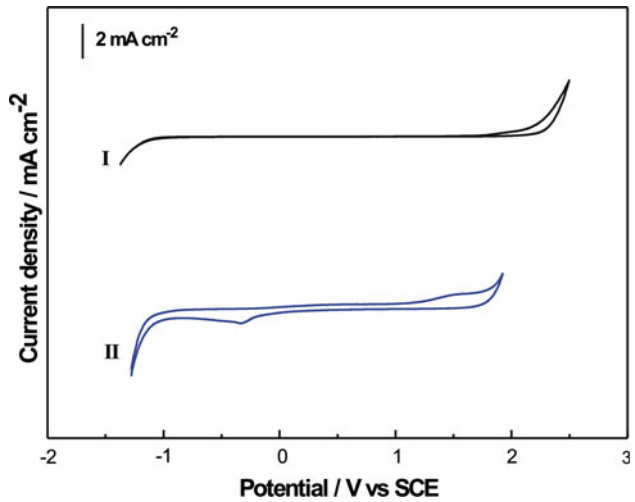

Fig. 3 Cyclic voltammograms in 0.1 M H_2SO_4 solution at the BDND film electrode (*curve I*) and glassy carbon electrode (*curve II*) at the scan rate of 50 mV s^{-1}

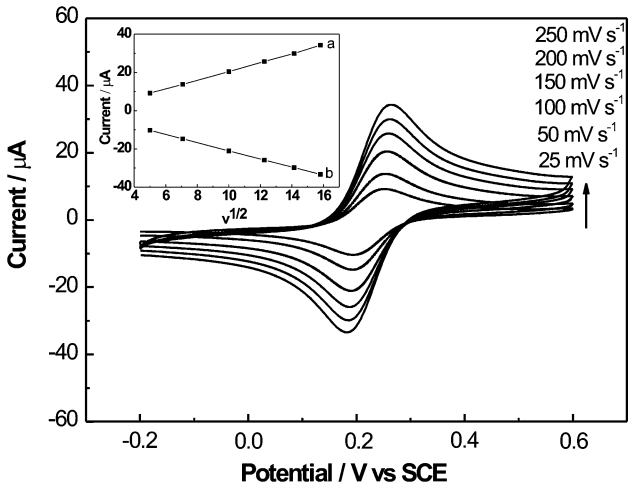

Fig. 4 Typical CV of 0.2 mM $K_3Fe(CN)_6$ in 1 M KCl solution at the BDND film electrode at the scan rate varying from 25 to 250 mV s^{-1}. The *insert* is the corresponding current-$v^{1/2}$ plots of the data

relative standard deviation (RSD) of 0.6 %, indicating that the electrode surface was not poisoned by the reaction intermediates and can be used repeatedly. Those results demonstrated that the BDND electrode possesses the promising features for analytical applications.

To address the disadvantage of enzymatic electrochemical sensors for glucose, non-enzymatic glucose sensors based on metal and diamond electrode were developed. In the present study, the detection of glucose in 0.1 M NaOH aqueous solution at the un-modified BDND film electrode and glassy carbon electrode were performed. Figure 6 shows the typical CV curves for the BDND film electrode and glassy carbon electrode in 0.1 M NaOH solution containing 5 mM glucose at the scan rate of 25 mV s^{-1}. It can be seen that glucose was easily oxidized and a well-defined current response for glucose was obtained at the BDND film electrode, as shown in the curve I in Fig. 6. There is an obvious peak at about 655 mV versus SCE during the forward and backward sweeping, which corresponds to the oxidation of glucose at the BDND film electrode. The peak current of backward sweep decreases slightly than that of forward sweep, which indicates that the BDND film electrode

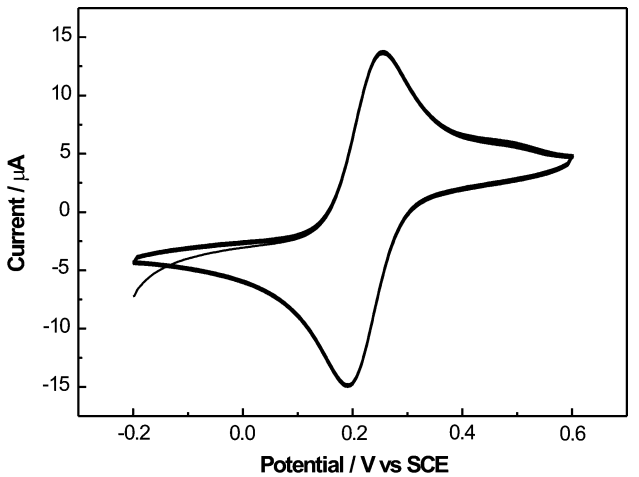

Fig. 5 Cyclic voltammograms of 0.2 mM $K_3Fe(CN)_6$ in 1 M KCl solution at the BDND film electrode for successive ten times scanning at the scan rate of 50 mV s^{-1}

has a strong pollution resistance. In the absence of glucose, the peak current was not observed. The similar electrochemical behaviors and detection of glucose on the metal-modified

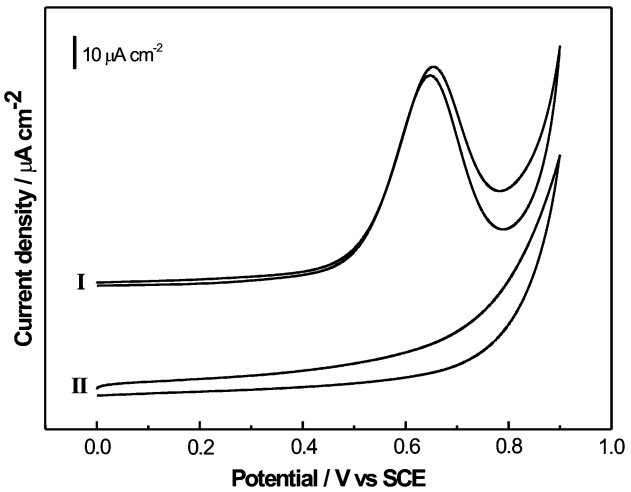

Fig. 6 Typical CV of 5 mM glucose in 0.1 M NaOH solution at the BDND film electrode (*curve I*) and glassy carbon electrode (*curve II*) at the scan rate of 25 mV s^{-1}

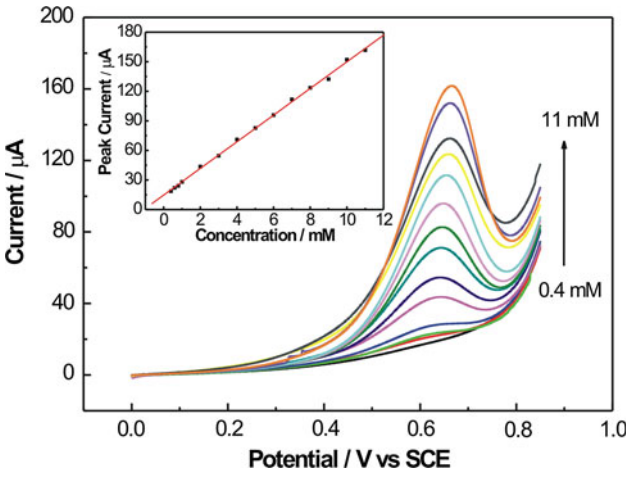

Fig. 7 Linear sweep voltammograms of different glucose concentrations in 0.1 M NaOH solution at the BDND film electrode at the scan rate of 25 mV s^{-1}. The *inset* is the relationship between the glucose concentrations and peak currents in the range of 0.4–11 mM

boron-doped diamond electrode and bare boron-doped diamond film electrode treated with the hydrogen flame were also observed [15, 20, 21]. In comparison with BDND film electrode, however, no visual oxidization peak on the CV curve (curve II) in Fig. 6 is observed at the glassy carbon electrode at the same measurement conditions. It demonstrated that glucose was readily oxidized at the boron-doped nanocrystalline diamond film electrodes. However, no glucose oxidization peak was observed at the glass carbon electrode. The similar results were also reported for the boron-doped nanocrystalline diamond and micro-crystalline diamond film electrode in the literature [16, 17]. Based on those results, it is indicated that the sp^2 carbon has no significant effect on oxidizing glucose under this condition. Therefore, it is suggested that the mechanism for glucose direct oxidation at boron-doped nanocrystalline diamond film electrodes was not similar to the model for anodic oxygen transfer reaction proposed by Swain and coworkers [32]. It was regarded that the mechanisms of direct oxidation of glucose on the boron-doped nanocrystalline diamond film electrode surface were associated with the doped boron atoms, which acted as the active sites in the glucose oxidation. Glucose was proposed to adsorb or coordinate at boron sites on the boron-doped nanocrystalline diamond film surface, and then be directly oxidized on the boron-doped nanocrystalline diamond film electrode [17].

Figure 7 shows a series of linear sweep voltammograms for the oxidation of glucose at various concentrations in 0.1 M NaOH solution at the BDND film electrode at the scan rate of 25 mV s^{-1}. The oxidation peak corresponding to the oxidation of glucose with concentration varying from 0.4 to 11 mM at about 655 mV versus SCE can be observed, and the peak current increases with the increase of glucose concentration, which indicated that glucose was easily oxidized at the BDND film electrode. The results demonstrated

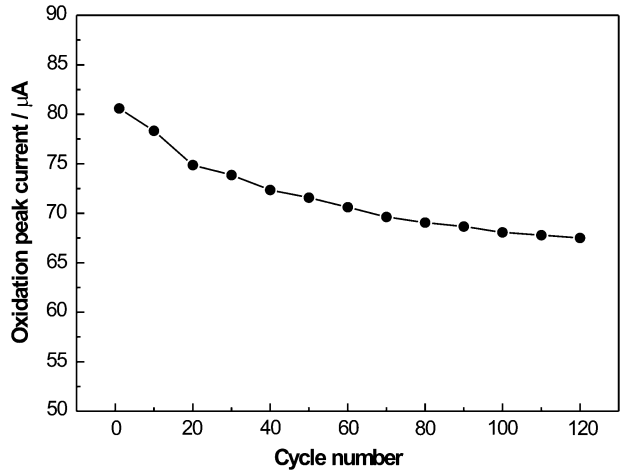

Fig. 8 The electrochemical cycling stability of the BDND film electrode for 5 mM glucose in 0.1 M sodium hydroxide solutions at the scan rate of 25 mV s^{-1}

that the peak current response of glucose is linear in the concentration range between 0.4 and 11 mM, which contains the glucose concentration range in human blood (about 3–8 mM), as shown in the inset of Fig. 7. The regression equation is i_p (μA) = 14.69 + 13.52C (mM), with the correlation coefficient (R) of 0.9993 and sensitivity of 30.05 μA mM^{-1} cm^{-2}. To investigate the repeatability and stability of BDND film electrode for 5 mM glucose in 0.1 M sodium hydroxide solutions, repetitive measurements of the CV detection were carried out at the scan rate of 25 mV s^{-1}. The loss of the electrochemical activity was about 16.2 % after 120 repetitive cycles according to the decrease of glucose oxidation peak current, as shown in Fig. 8, indicating that BDND film electrode was relatively stable owing to its inertness of the diamond surface.

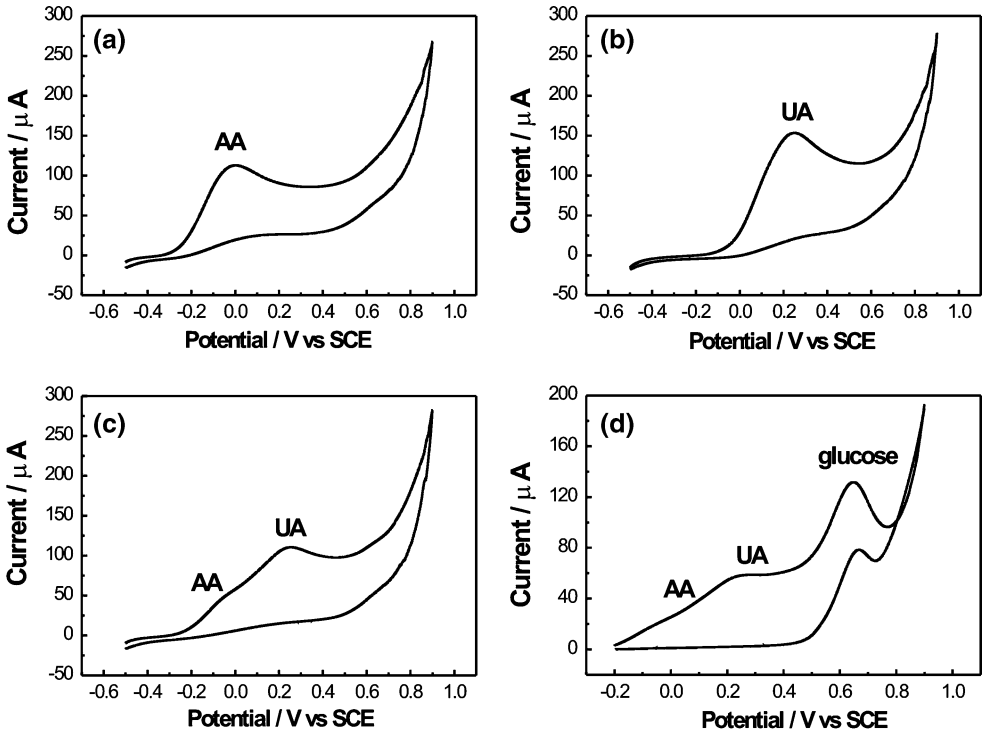

Fig. 9 Cyclic voltammograms of (**a**) 2 mM AA; (**b**) 2 mM UA; (**c**) the mixture of 1 mM AA and 1 mM UA; (**d**) the mixture of 0.5 mM AA, 0.5 mM UA, and 5 mM glucose at the BDND film electrode. The supporting electrolyte and the scan rate are 0.1 M NaOH solution and 25 mV s^{-1}, respectively

The interference of some potentially interfering organism to the electrochemical signal is the major challenge of non-enzymatic glucose sensor in application. UA and AA are known to interfere with electrochemical glucose detection in both enzyme-based sensors and direct amperometric sensors, which are also simultaneously oxidized along with glucose at the electrode surface, resulting in the interfering electrochemical signals. Therefore, the electrochemical measurements for the interfering species (AA and UA) were also carried out in 0.1 M NaOH aqueous solutions at the BDND electrode. Figure 9a–c shows the linear sweep voltammograms of AA, UA, and a mixture of UA and AA at BDND film electrodes, respectively. From Fig. 9a, b, it can be seen that AA and UA interference compounds are oxidized at about 5 and 250 mV versus SCE, respectively. A weak voltammetric signal at about 5 mV and a strong voltammetric signal at about 250 mV were observed for the mixture of 1 mM UA and 1 mM AA, which indicated that the BDND film electrode can separate AA and UA. Figure 9d shows the linear sweep voltammograms of glucose containing AA and UA at BDND film electrode. The concentration of glucose was 5 mM, while the concentrations of AA and UA were both 0.5 mM, which is above the physiological concentration of about 0.1 mM. The electrochemical oxidation peak is clearly separated in the presence of AA and UA. A well-defined peak of glucose oxidation at about 655 mV was obtained, and the oxidation peak of AA and UA did not overlap with the glucose oxidation peak. These results suggest that the selective detection of glucose can be achieved at the BDND film electrode in the presence of interfering species of AA and UA.

4 Conclusions

BDND films were deposited by MWCVD system in a gas mixture of CH_4/H_2/TMB. The introduction of boron atoms resulted in the grains gathering together and forming ball-like clusters with inhomogeneous size. The BDND film electrode showed wide potential window, fast electron transfer, and good reversibility and repeatability of electrode reaction. The non-enzymatic glucose sensor based on the as-prepared BDND film electrode without any modification was developed. The results demonstrated that glucose could be directly oxidized, and the peak current is proportional to the glucose concentration in the range of 0.4–11.0 mM with a correlation coefficient of 0.9993 and sensitivity of 30.05 μA mM^{-1} cm^{-2}. The voltammetric signal of glucose and the mixture of AA and UA can be observed and well-separated at BDND film electrodes, and glucose can be selectively detected in the presence of UA and AA in alkaline solution using the as-prepared BDND film electrode.

Acknowledgments This work was financially supported by the National Nature Science Foundation of China (51002078 and 61222403), the Fundamental Research Funds for the Central Universities (No. 30920130111019, 30920130111017, and NE2012004), the

QingLan Project of Jiangsu Province, the Natural Science Foundation of Jiangsu Province of China (BK2011709), Doctoral Program Foundation of Ministry of Education of China (No. 20123218110030), and the opened fund of the state key laboratory on integrated optoelectronics (No. IOSKL2012KF06).

References

1. Denisenko A, Kohn E (2005) Diamond power devices: concepts and limits. Diam Relat Mater 14:491–498
2. Rao TN, Fujishima A (2009) Recent advances in electrochemistry of diamond. Diam Relat Mater 9:384–389
3. Compton RG, Foord JS, Marken F (2003) Electroanalysis at diamond-like and doped-diamond electrodes. Electroanalysis 15:1349–1363
4. Lasseter TL, Clare BH, Abbott NL, Hamers RJ (2004) Covalently modified silicon and diamond surfaces: resistance to nonspecific protein adsorption and optimization for biosensing. J Am Chem Soc 126:10220–10221
5. Tatsuma T, Mori H, Fujishima A (2000) Electron transfer from diamond electrodes to hemepeptide and peroxidase. Anal Chem 72:2919–2924
6. Zhao GH, Li PQ, Nong FQ, Li MF, Gao JX, Li DM (2010) Construction and high performance of a novel modified boron-doped diamond film electrode endowed with superior electrocatalysis. J Phys Chem C 114:5906–5908
7. Zhou YL, Tian RH, Zhi JF (2007) Amperometric biosensor based on tyrosinase immobilized on a boron-doped diamond electrode. Biosens Bioelectron 22:822–828
8. Yang WS, Auciello O, Butler JE, Cai W, Carlisle JA, Gerbi J, Gruen DM, Knickerbocker T, Lasseter TL, Russell JN, Simith LM, Hamers RJ (2002) DNA-modified nanocrystalline diamond thin-films as stable, biologically active substrates. Nat Mater 1:253–257
9. Yang NJ, Uetsuka H, Nebel CE (2009) Biofunctionalization of vertically aligned diamond nanowires. Adv Funct Mater 19: 887–893
10. Deng CY, Chen JH, Chen XL, Xiao CH, Nie LH, Yao SZ (2008) Direct electrochemistry of glucose oxidase and biosensing for glucose based on boron-doped carbon nanotubes modified electrode. Biosens Bioelectron 23:1272–1277
11. Loh KP, Zhao SL, Zhang WD (2004) Diamond and carbon nanotube glucose sensors based on electropolymerization. Diam Relat Mater 13:1075–1079
12. Zhao W, Xu JJ, Qiu QQ, Chen HY (2006) Nanocrystalline diamond modified gold electrode for glucose biosensing. Biosens Bioelectron 26:649–655
13. Wang J, Carlisle JA (2006) Covalent immobilization of glucose oxidase on conducting ultrananocrystalline diamond thin films. Diam Relat Mater 15:279–284
14. Bao SJ, Li CM, Zang JF, Cui XQ, Qiao Y, Guo J (2008) New nanostructured TiO_2 for direct electrochemistry and glucose sensor applications. Adv Funct Mater 18:591–594
15. Watanabe T, Ivandini TA, Makide Y, Fujishima A, Einaga Y (2006) A selective detection method derived from controlled diffusion process at metal-modified diamond electrodes. Anal Chem 78:7857–7860
16. Zhao JW, Wu DH, Zhi JF (2009) A direct electrochemical method for diabetes diagnosis based on as-prepared boron-doped nanocrystalline diamond thin film electrodes. J Electroanal Chem 626:98–102
17. Zhao JW, Wu LZ, Zhi JF (2009) Non-enzymatic glucose detection using as-prepared boron-doped diamond thin-film electrodes. Analyst 134:794–799
18. Luo DB, Wu LZ, Zhi JF (2009) Fabrication of boron-doped diamond nanorod forest electrodes and their application in non-enzymatic amperometric glucose biosensing. ACS NANO 3:2121–2128
19. Cui HF, Ye JS, Zhang WD, Li CM, Luong JHT, Sheu FS (2007) Selective and sensitive electrochemical detection of glucose in neutral solution using platinum–lead alloy nanoparticle/carbon nanotube nanocomposites. Anal Chim Acta 594:175–183
20. Lee JW, Park SM (2005) Direct electrochemical assay of glucose using boron-doped diamond electrodes. Anal Chim Acta 545:27–32
21. Ivandini TA, Sato R, Makide Y, Fujishima A, Einaga Y (2004) Electroanalytical application of modified diamond electrodes. Diam Relat Mater 13:2003–2008
22. Jiang LC, Zhang WD (2010) A highly sensitive nonenzymatic glucose sensor based on CuO nanoparticles-modified carbon nanotube electrode. Biosens Bioelectron 25:1402–1407
23. Yang GC, Liu E, Khun NW, Jiang SP (2009) Direct electrochemical response of glucose at nickel-doped diamond like carbon thin film electrodes. J Electroanal Chem 627:51–57
24. Wilson R, Turner APF (1992) Glucose oxidase: an ideal enzyme. Biosens Bioelectron 7:165–185
25. Yang J, Zhang WD, Gunasekaran S (2010) An amperometric non-enzymatic glucose sensor by electrodepositing copper nanocubes onto vertically well-aligned multi-walled carbon nanotube arrays. Biosens Bioelectron 26:279–284
26. Zhuang Z, Su X, Yuan H, Sun Q, Xiao D, Choi MMF (2008) An improved sensitivity non-enzymatic glucose sensor based on a CuO nanowire modified Cu electrode. Analyst 133:126–132
27. Park S, Boo H, Chung TD (2006) Electrochemical non-enzymatic glucose sensors. Anal Chim Acta 556:46–57
28. Salimi A, Roushani M (2005) Non-enzymatic glucose detection free of ascorbic acid interference using nickel powder and nafion sol–gel dispersed renewable carbon ceramic electrode. Electrochem Commun 7:879–887
29. Yuan JH, Wang K, Xia XH (2005) Highly ordered platinum-nanotubule arrays for amperometric glucose sensing. Adv Funct Mater 15:803–809
30. Wang YG, Lau SP, Tay BK, Zhang XH (2002) Resonant Raman scattering studies of Fano-type interference in boron doped diamond. J Appl Phys 92:7253–7256
31. Bernard M, Deneuville A, Muret P (2004) Non-destructive determination of the boron concentration of heavily doped metallic diamond thin films from Raman spectroscopy. Diam Relat Mater 13:282–286
32. Koppang MD, Witek M, Blau J, Swain GM (1999) Electrochemical oxidation of polyamines at diamond thin-film electrodes. Anal Chem 71:1188–1195